J. Fluid Mech. (2011), *vol.* 689, *pp.* 183–202.
doi:10.1017/jfm.2011.410

Finite wavelength selection for the linear instability of a suspension of settling spheroids

Anders A. Dahlkild†

Linné Flow Centre, Department of Mechanics, KTH, 100 44 Stockholm, Sweden

(Received 22 February 2011; revised 16 June 2011; accepted 15 September 2011;
first published online 7 November 2011)

The instability of an initially homogeneous suspension of spheroids, settling due to gravity, is reconsidered. For non-spherical particles, previous studies in the literature report that normal-mode density perturbations of maximum growth rate are those of arbitrarily large, horizontal wavelength. Using the 'mixture theory' for two-phase flow we show that the maximum growth rate for horizontal density perturbations is obtained for a finite wavelength if the inertia of the bulk motion associated with the normal-mode density perturbation is accounted for. We find that for long wavelengths, $\lambda \to \infty$, the growth rate approaches zero as $\lambda^{-2/3}$. The maximum growth rate is obtained for $\lambda \sim d/\sqrt{\alpha_0 Re_L^{1/2}}$, where d is the axis perpendicular to the axis of rotational symmetry of the spheroid, α_0 is the undisturbed volume fraction of particles and Re_L, typically $\ll 1$, is a Reynolds number of the bulk motion on a typical length scale $L \sim d/\sqrt{\alpha_0}$ and a velocity scale on the order of the undisturbed settling speed. The theoretical results for the wavelength selection agree qualitatively well with previous experimental results in the literature of measured correlation lengths of vertical streamers in settling fibre suspensions.

Key words: instability, particle/fluid flow, suspension

1. Introduction

An unresolved theoretical issue in the area of settling particle suspensions is the prediction of the length scale of so-called vertical streamers observed experimentally in suspensions of elongated particles or fibres at low particle Reynolds number. Metzger, Butler & Guazzelli (2007*a*) report the formation of alternating regions of vertical streamers and back-flow, which in the early development span the height of the container. Earlier studies, by Kumar & Ramaro (1991) and Herzhaft & Guazzelli (1999), also report similar phenomena, leading to an enhanced settling rate of the particles as compared to their single-particle settling speed. Metzger, Guazzelli & Butler (2005) find that the vertical structures evolved with time from long wavelengths, comparable to the container width, towards shorter ones but without reaching a true steady state. Metzger *et al.* (2007*a*), hereafter referred to as MBG, extend the experimental study by Metzger *et al.* (2005) to see how the wavelength selection depends on container size. They find that for containers that are large enough the most unstable wavelength is independent of and less than the width of the container.

† Email address for correspondence: ad@mech.kth.se

Also, within their experimental accuracy the most unstable wavelength is essentially independent of volume fraction and basic properties of the fibres and the fluid.

However, as noted by MBG, no theory so far has been able to predict the wavelength selection in an initially homogeneous suspension of fibres. Available linear instability theory by Koch & Shaqfeh (1989) finds that the fastest-growing wave is that of infinite wavelength. They suggest that wavelengths of the order $(nl)^{-1/2}$, where n is the particle number density and l is the fibre length, will in the end predominate due to nonlinear effects. Neither of these theories is confirmed in the experiments by MBG. Numerical simulations for interacting, settling fibres at zero Reynolds number using periodic boundary conditions are reported by e.g. Mackaplow & Shaqfeh (1998), Butler & Shaqfeh (2002), Saintillian, Darve & Shaqfeh (2005), Saintillian, Shaqfeh & Darve (2006*a*) and Tornberg & Gustavsson (2006). They all find the formation of a single streamer as restricted by the size of the computational cell. In simulations of the same kind, but including the bottom wall of the container, Saintillian *et al.* (2006*a*) show that an initial single streamer continuously breaks down into smaller structures as time proceeds, in qualitative agreement with the experiments of Metzger *et al.* (2005). The linear instability analysis of Saintillian, Shaqfeh & Darve (2006*b*) demonstrates that this evolution in time of the structures' size may be attributed to the development of a background stratification in the suspension. However, Metzger, Butler & Guazzelli (2007*b*) tested this idea and found that it does not account for the length scale reduction observed experimentally. The effect of finite particle Reynolds number is investigated by Kuusela, Lahtinen & Ala-Nissila (2005) and Shin, Koch & Subramanian (2009), but still the wavelength selection is not yet resolved, as also concluded by Guazzelli & Hinch (2011) in a recent review on the subject. (For a more detailed description of background information to the problem we recommend the paper by Metzger *et al.* 2007*a* and the review by Guazzelli & Hinch 2011, including supplementary movie material.)

In the present paper we suggest a mechanism for wavelength selection in an initially homogeneous suspension by extending the theory of Koch & Shaqfeh (1989), hereafter referred to as KS. The basic mechanism for the instability is described in detail by KS. A density perturbation is reinforced as the fibres settle sideways into regions of high density when the fibres orient themselves in the principal direction of fluid deformation as a result of the flow induced by the density perturbation. This physical mechanism is still predominating in our theory presented here. However, we extend the analysis by accounting for the inertia of the bulk flow in the streamers/back-flow. Effects of inertia will then be of particular importance for large wavelengths, as then viscous forces are small and the gravity force from the density perturbation is rather balanced by inertia. This inertia decreases the magnitude of the columnar shear flow motion that aligns the fibres, whereby the growth rate is substantially lower at small wavenumbers as compared to the theory by KS. The new theory is finally applied to the experimental conditions studied by MBG to verify the wavelength selection predicted. The results should be of generic importance in similar sedimentation problems where a sideways settling component is present and coupled to the bulk flow, as e.g. in the case of lateral drift of bubbles, as recently studied by Narsimhan & Shaqfeh (2010), as well as serving as a guide for future experiments.

2. Formulation

2.1. *Motion of the mixture*

Settling due to gravity of a dilute, monodispersed suspension of spheroids at an overall average volume fraction α_0 is considered. The continuous liquid phase is denoted by C and the dispersed phase by D. If the local volume fraction of spheroids is α, the

density of the mixture is

$$\rho = \alpha\rho_D + (1-\alpha)\rho_C. \tag{2.1}$$

We use the 'mixture formulation' (see for example Ishii 1975; Ungarish 1993) of two-phase flow, where the mixture of the two phases as a whole is treated as one single effective fluid, of which the physical properties such as viscosity and density depend on the local volume fraction of the dispersed phase. In commercial computational flow solvers this model of two-phase flow is often referred to as the 'algebraic slip' model. The local average relative velocity of the dispersed phase $\boldsymbol{v}_R$ (settling speed) is then assumed to be given by some algebraic relationship dependent on the physical properties of the suspension. The evolution of the particle volume fraction is determined from a conservation equation of the dispersed phase that accounts for its motion relative to the bulk fluid. This formulation thus assumes a quasi-steady state of the particles' relative motion (i.e. small Stokes number), and neglects inertia of the fluid–particle relative flow, which magnitude is typically much lower than that of the bulk motions in the effective fluid. The mass-averaged velocity of the mixture, $\boldsymbol{u}$, is defined by

$$\rho\boldsymbol{u} = \rho_D\alpha\boldsymbol{v}_D + \rho_C(1-\alpha)\boldsymbol{v}_C, \tag{2.2}$$

where $\boldsymbol{v}_D$ and $\boldsymbol{v}_C$ are the separate velocities of the dispersed and continuous phases respectively. The volume-averaged velocity can be written

$$\boldsymbol{j} = \alpha\boldsymbol{v}_D + (1-\alpha)\boldsymbol{v}_C. \tag{2.3}$$

Let $\boldsymbol{v}_R$ denote the relative velocity of the dispersed phase

$$\boldsymbol{v}_R = \boldsymbol{v}_D - \boldsymbol{j}. \tag{2.4}$$

Then $\boldsymbol{u}$ and $\boldsymbol{j}$ are related by

$$\boldsymbol{j} = \boldsymbol{u} - \frac{\epsilon\alpha}{1+\epsilon\alpha}\boldsymbol{v}_R, \tag{2.5}$$

where ϵ is the relative density difference

$$\epsilon = \frac{\rho_D - \rho_C}{\rho_C}. \tag{2.6}$$

For an idealized one-dimensional settling process in a vertical vessel of a stagnant homogeneous, stable suspension one would have $\boldsymbol{j} = 0$, and $\boldsymbol{u} = (\epsilon\alpha/(1+\epsilon\alpha))\boldsymbol{v}_R$ then represents the superficial mass transport of the settling particles due to their relative motion. The algebraic relationship for the local average relative velocity $\boldsymbol{v}_R$, or settling speed, will be specified later. Bulk motions of the mixture may appear as a result of buoyancy due to an inhomogeneous particle distribution $\alpha(\boldsymbol{x}, t)$. Conservation of momentum and volume of the mixture requires

$$\rho(\alpha)\left(\frac{\partial\boldsymbol{u}}{\partial t} + \boldsymbol{u}\cdot\nabla\boldsymbol{u}\right) = -\nabla P + (\rho(\alpha) - \rho(\alpha_0))\boldsymbol{g} + \nabla\cdot\left[\mu_e\left(\nabla\boldsymbol{u} + \nabla\boldsymbol{u}^T - \frac{2}{3}\boldsymbol{I}\,\nabla\cdot\boldsymbol{u}\right)\right], \tag{2.7}$$

$$\nabla\cdot\boldsymbol{u} = \nabla\cdot\left(\frac{\epsilon\alpha}{1+\epsilon\alpha}\boldsymbol{v}_R\right), \tag{2.8}$$

where $P = p - \rho(\alpha_0)\boldsymbol{g}\cdot\boldsymbol{x}$ is the reduced pressure. The effective viscosity of the mixture, μ_e, generally depends on the particle volume fraction, the local orientational state of the spheroids and possibly also on the local shear rate of the mixture. Here, we shall simply take the viscosity as constant, $\mu_e = \mu_C$, which should prevail approximately in the dilute limit considered here. Conservation of particle volume requires

$$\frac{\partial \alpha}{\partial t} + \nabla\cdot(\alpha \boldsymbol{v}_D) = \frac{\partial \alpha}{\partial t} + \nabla\cdot(\alpha \boldsymbol{j} + \alpha \boldsymbol{v}_R) = 0. \tag{2.9}$$

However, the equations above do not form a closed set of equations since the average relative speed, $\boldsymbol{v}_R$, is dependent on the local orientational distribution of the spheroids. The orientational distribution of particles may continuously change as a result of the mixture bulk motion. Thus (2.9) must be replaced with an equation describing the evolution of the particles position in parallel with their orientation, as discussed in the following subsection.

2.2. *Motions of the spheroids*

Under Stokes flow conditions the settling velocity of a single isolated spheroid is given by (Happel & Brenner 1965)

$$\boldsymbol{v}_s(\boldsymbol{p}) = (V_{s,\parallel} - V_{s,p})\boldsymbol{e}_g + V_{s,p}(\boldsymbol{e}_g\cdot\boldsymbol{p})\boldsymbol{p}. \tag{2.10}$$

Here, $V_{s,\parallel}$ is the settling velocity of a spheroid oriented parallel to the direction of gravity, and $V_{s,p}$ is the complementary drift velocity along the orientation vector $\boldsymbol{p}$ according to (2.10). These velocities can be written

$$V_{s,\parallel} = \frac{\epsilon g l^2}{\nu_C}\gamma_0(r), \quad V_{s,p} = \frac{\epsilon g l^2}{\nu_C}\gamma_1(r), \tag{2.11}$$

where l is the length of the spheroid, ν_C is the kinematic viscosity of the suspending liquid, and $\gamma_0(r)$ and $\gamma_1(r)$ are functions of the aspect ratio of the spheroid, $r = l/d$. The complete expressions are lengthy and not given here. For large aspect ratios, though, one finds the leading-order terms

$$\gamma_0(r) \approx \frac{2\ln(2r) - 1}{24r^2}, \quad \gamma_1(r) \approx \frac{\ln(2r) - 1.5}{24r^2}. \tag{2.12}$$

Slender-body theory for rod particles (Batchelor 1970) gives a similar result,

$$\gamma_0(r) \approx \frac{2\ln(2r) - 1.614}{16r^2}, \quad \gamma_1(r) \approx \frac{\ln(2r) - 1.807}{16r^2}, \tag{2.13}$$

for which the analysis is equally valid. Equation (2.10) is also taken as the instantaneous relative velocity of a spheroid in a local bulk flow of the mixture. In addition, the motions in the bulk may change the orientation vector $\boldsymbol{p}$ of the spheroid. Again, assuming Stokes flow conditions, we can superpose the rotational motion of the spheroid according to Jeffrey (1922) as given by the local strain and rotation rates of the bulk flow:

$$\dot{\boldsymbol{p}} = \boldsymbol{W}\cdot\boldsymbol{p} + \Gamma\left[\boldsymbol{E}\cdot\boldsymbol{p} - \boldsymbol{E} : (\boldsymbol{p}\boldsymbol{p}^T)\boldsymbol{p}\right], \quad \Gamma = \frac{r^2 - 1}{r^2 + 1}, \tag{2.14}$$

where

$$\boldsymbol{E} = \tfrac{1}{2}\left(\nabla\boldsymbol{u} + \nabla\boldsymbol{u}^T\right), \quad \boldsymbol{W} = \tfrac{1}{2}\left(\nabla\boldsymbol{u}^T - \nabla\,\boldsymbol{u}\right). \tag{2.15}$$

To consider the collection of spheroids in the suspension we use a statistical approach. Let the local volume fraction of particles at position $\boldsymbol{x}$ with orientation vector $\boldsymbol{p}$ within the space angle $\mathrm{d}\Omega(\boldsymbol{p})$ be $\alpha_0\Psi(\boldsymbol{x},\boldsymbol{p},t)\,\mathrm{d}\Omega(\boldsymbol{p})/4\pi$, where Ψ is the normalized density of particles in physical and orientational space. The local particle volume fraction irrespective of orientation is then obtained from

$$\alpha(\boldsymbol{x},t)=\frac{\alpha_0}{4\pi}\int_\Omega \Psi(\boldsymbol{x},\boldsymbol{p},t)\,\mathrm{d}\Omega(\boldsymbol{p}). \tag{2.16}$$

We assume the volume fraction small enough that it is meaningful to approximate the collective settling and rotational motions of hydrodynamically interacting spheroids with those of the single spheroid motions given above. The local translational velocity of a single spheroid at orientation $\boldsymbol{p}$ is then

$$\boldsymbol{v}_D(\boldsymbol{x},\boldsymbol{p},t)=\boldsymbol{j}(\boldsymbol{x},t)+\boldsymbol{v}_s(\boldsymbol{p}), \tag{2.17}$$

and the average velocity of the dispersed phase

$$\boldsymbol{v}_D(\boldsymbol{x},t)=\boldsymbol{j}(\boldsymbol{x},t)+\boldsymbol{v}_R(\boldsymbol{x},t), \tag{2.18}$$

where

$$\left.\begin{aligned}\boldsymbol{v}_D(\boldsymbol{x},t)&=\frac{\dfrac{1}{4\pi}\displaystyle\int_\Omega \boldsymbol{v}_D(\boldsymbol{x},\boldsymbol{p},t)\Psi(\boldsymbol{x},\boldsymbol{p},t)\,\mathrm{d}\Omega(\boldsymbol{p})}{\dfrac{1}{4\pi}\displaystyle\int_\Omega \Psi(\boldsymbol{x},\boldsymbol{p},t)\,\mathrm{d}\Omega(\boldsymbol{p})},\\ \boldsymbol{v}_R(\boldsymbol{x},t)&=\frac{\dfrac{1}{4\pi}\displaystyle\int_\Omega \boldsymbol{v}_s(\boldsymbol{p})\Psi(\boldsymbol{x},\boldsymbol{p},t)\,\mathrm{d}\Omega(\boldsymbol{p})}{\dfrac{1}{4\pi}\displaystyle\int_\Omega \Psi(\boldsymbol{x},\boldsymbol{p},t)\,\mathrm{d}\Omega(\boldsymbol{p})}.\end{aligned}\right\} \tag{2.19}$$

The conservation of spheroids in physical and orientational space is expressed by the Fokker–Planck equation,

$$\frac{\partial}{\partial t}\Psi(\boldsymbol{x},\boldsymbol{p},t)+\nabla\cdot[\boldsymbol{v}_D(\boldsymbol{x},\boldsymbol{p},t)\Psi(\boldsymbol{x},\boldsymbol{p},t)]+\nabla_p\cdot[\dot{\boldsymbol{p}}(\boldsymbol{x},\boldsymbol{p},t)\Psi(\boldsymbol{x},\boldsymbol{p},t)]=0, \tag{2.20}$$

where ∇_p is the gradient operator in orientational space. (Integration of (2.20) over all space angles results in (2.9).) This completes the set of equations governing the motion of the mixture and the evolution of the particle distribution in physical as well in orientational space within the framework of 'mixture theory'.

2.3. *Motions in a plane horizontal wave*

In the development of the description of motion of the spheroids we considered a suspension in the dilute limit $\alpha \ll 1$. (A more precise restriction for particles of large aspect ratios is that $\alpha r^2 \ll 1$.) Thus, as in many settling processes we shall assume here also that the relative increase of the mixture density due to the presence of the particles is small, i.e. $\epsilon\alpha \ll 1$. Therefore, the difference between $\boldsymbol{u}$ and $\boldsymbol{j}$ in (2.5) is neglected in the following as well as the right-hand side of (2.8).

Then, to study the instability of the suspension we consider the development of a plane horizontal wave, which was found by Koch & Shaqfeh (1989) to have the largest growth rate. Physically this is a natural result since the density gradient of the perturbation is then perpendicular to the gravitational force. Let the x-axis be vertical in the direction of gravity, let the y-axis be in the direction of the wavenumber vector

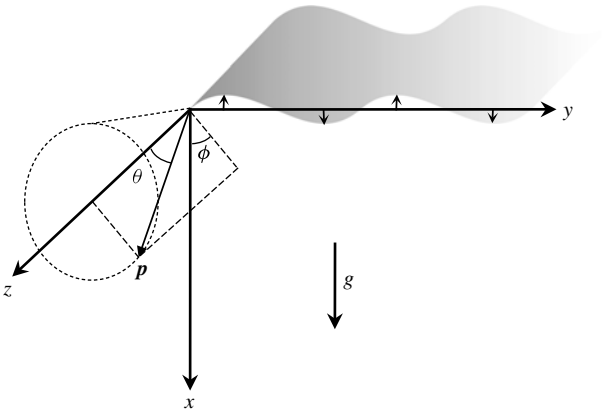

FIGURE 1. Definition of coordinate system.

and let the z-axis be in the other horizontal direction. The dependent variables then depend only on one variable in physical space, y. Also, we may assume the horizontal components of the bulk velocity to be zero, $\boldsymbol{u} = u(y,t)\boldsymbol{e_x}$. The orientation vector $\boldsymbol{p}$ is expressed in terms of the azimuthal, θ and polar, ϕ, angles of the spherical coordinates on a unit sphere, $\boldsymbol{p} = (\sin\theta\,\cos\phi, \sin\theta\,\sin\phi, \cos\theta)^{\mathrm{T}}$. The rotational motions of the spheroids according to (2.14) then reduce to

$$\dot{\boldsymbol{p}} = \sin\theta\,\dot{\phi}\,\boldsymbol{e_\phi} + \dot{\theta}\,\boldsymbol{e_\theta}, \tag{2.21}$$

$$\dot{\phi} = \frac{1}{2}\,(\Gamma\,\cos\,2\phi - 1)\,\frac{\partial u}{\partial y}, \quad \dot{\theta} = \frac{\Gamma}{4}\,\sin\,2\theta\,\sin\,2\phi\,\frac{\partial u}{\partial y}, \tag{2.22}$$

where $\boldsymbol{e_\phi} = (-\sin\phi, \cos\phi, 0)^{\mathrm{T}}$ and $\boldsymbol{e_\theta} = (\cos\theta\,\cos\phi, \cos\theta\,\sin\phi, -\sin\theta)^{\mathrm{T}}$ are unit vectors of the spherical coordinate system. The translational motion of the spheroids in the horizontal direction is given by (2.17) and (2.10):

$$v_{D,y} = \boldsymbol{v}_s \cdot \boldsymbol{e_y} = V_{s,p}(\boldsymbol{e_g}\cdot\boldsymbol{p})\,\boldsymbol{p}\cdot\boldsymbol{e_y} = \frac{V_{s,p}}{2}\sin^2\theta\,\sin 2\phi. \tag{2.23}$$

We introduce non-dimensional variables using a velocity scale $V_s = (1/3)V_{s,p}$ for the dispersed phase and V_s/Γ for the mixture. A length scale is obtained from the balance of viscous forces and buoyancy in the momentum equation of the mixture

$$L = \sqrt{\frac{\nu_C V_s/\Gamma}{\epsilon\alpha_0 g}} = l\sqrt{\frac{\gamma_1(r)/\Gamma}{3\alpha_0}} \approx l\sqrt{\frac{\ln(2r)}{72\alpha_0 r^2}}, \tag{2.24}$$

where α_0 is the initial, homogeneous volume fraction of particles. A time scale is then given by L/V_s. The inverse of the chosen length scale is, as we shall see in detail later, exactly the upper limit of the wavenumber for normal-mode exponential growth. The non-dimensional equations for conservation of momentum and particles are then

$$Re_L\frac{\partial\hat{u}}{\partial\hat{t}} = -\frac{\mathrm{d}\hat{P}}{\mathrm{d}\hat{x}} + \left(\frac{\alpha(\hat{y},\hat{t})}{\alpha_0} - 1\right) + \frac{\partial^2\hat{u}}{\partial\hat{y}^2}, \tag{2.25}$$

$$\frac{\partial\Psi}{\partial\hat{t}} + \frac{\partial}{\partial\hat{y}}\left(\hat{v}_{s,y}\Psi\right) + \frac{\partial}{\partial\phi}\left(\dot{\hat{\phi}}\Psi\right) + \frac{1}{\sin\theta}\frac{\partial}{\partial\theta}\left(\sin\theta\,\dot{\hat{\theta}}\,\Psi\right) = 0, \tag{2.26}$$

where

$$\hat{v}_{s,y} = \tfrac{3}{2}\sin^2\theta\ \sin 2\phi,$$
$$\dot{\hat{\phi}} = \frac{1}{2}\left(\cos 2\phi - \frac{1}{\Gamma}\right)\frac{\partial \hat{u}}{\partial \hat{y}}, \quad \dot{\hat{\theta}} = \frac{1}{4}\sin 2\theta\ \sin 2\phi \frac{\partial \hat{u}}{\partial \hat{y}}, \tag{2.27}$$

and where

$$\frac{\alpha(\hat{y},\hat{t})}{\alpha_0} = \frac{1}{2\pi}\int_{-\frac{\pi}{2}}^{\frac{\pi}{2}}\int_0^{\pi} \Psi(\theta,\phi,\hat{t})\ \sin\theta\,\mathrm{d}\theta\mathrm{d}\phi. \tag{2.28}$$

Due to symmetry of the spheroid particles it is sufficient here to consider orientations on half the unit sphere with $\theta \in [0,\pi]$ and $\phi \in [-\pi/2, \pi/2]$. The Reynolds number, defined by

$$Re_L = \frac{V_s L}{\nu_C}, \tag{2.29}$$

estimates the relative importance of inertial forces in a bulk motion of length scale L and a velocity of the order of the settling speed of the particles. Thus, although we neglect inertial effects of the particles' relative motion, $Re_d = V_s d/\nu_C \to 0$, inertia of the bulk motion is still accounted for.

3. Analysis

3.1. *Normal-mode analysis*

Following the result of Koch & Shaqfeh (1989), we look for exponentially growing non-travelling wave perturbations on a uniform, stagnant suspension of the form

$$\hat{u} = \hat{u}'(\hat{k})\,\mathrm{e}^{\hat{\sigma}\hat{t}+\mathrm{i}\hat{k}y}, \quad \Psi = 1 + \Psi'(\hat{k},\theta,\phi)\mathrm{e}^{\hat{\sigma}\hat{t}+\mathrm{i}\hat{k}y}, \tag{3.1}$$

where $\hat{u}', \Psi' \ll 1$ and the non-dimensional growth rate and wavenumber are

$$\hat{\sigma} = \frac{\sigma L}{V_s}, \quad \hat{k} = \frac{2\pi L}{\lambda}. \tag{3.2}$$

We realize that the reduced pressure gradient must be zero and cannot be part of the horizontal wave perturbation. Inserting (3.1) into (2.25)–(2.28) and collecting linear terms of the perturbation quantities give

$$(Re_L\hat{\sigma} + \hat{k}^2)\,\hat{u}'(\hat{k}) = \overline{\Psi}'(\hat{k}), \tag{3.3}$$
$$\left(\hat{\sigma} + \mathrm{i}\hat{k}\,\hat{v}_{s,y}(\theta,\phi)\right)\Psi'(\hat{k},\theta,\phi) = \mathrm{i}\hat{k}\,\tfrac{3}{2}\sin^2\theta\ \sin 2\phi\,\hat{u}'(\hat{k}), \tag{3.4}$$

where

$$\overline{\Psi}'(\hat{k}) = \frac{1}{2\pi}\int_{-\frac{\pi}{2}}^{\frac{\pi}{2}}\int_0^{\pi}\Psi'(\hat{k},\theta,\phi)\ \sin\theta\,\mathrm{d}\theta\mathrm{d}\phi \tag{3.5}$$

is the arbitrary, relative amplitude of the small perturbation of the volume fraction of particles. From (3.3), (3.4) and, for brevity, by identifying $\hat{v}_{s,y}$ on the right-hand side of (3.4) with the help of (2.27), one obtains for $\hat{u}'$ and Ψ' separately that

$$\hat{u}'(\hat{k}) = \frac{\overline{\Psi}'(\hat{k})}{Re_L\hat{\sigma} + \hat{k}^2}, \tag{3.6}$$

$$\Psi'(\hat{k},\theta,\phi) = \frac{\overline{\Psi}'(\hat{k})}{Re_L\hat{\sigma}+\hat{k}^2}\,\frac{[\hat{k}\,\hat{v}_{s,y}(\theta,\phi)]^2 + \mathrm{i}\hat{\sigma}\hat{k}\,\hat{v}_{s,y}(\theta,\phi)}{\hat{\sigma}^2+[\hat{k}\,\hat{v}_{s,y}(\theta,\phi)]^2}. \tag{3.7}$$

One may note that as $\hat{\sigma}$ is real, Ψ' has one contribution which is in phase with $\hat{u}'$, whereas the phase of the second contribution is a quarter of a wavelength before that of $\hat{u}'$. The in-phase contribution corresponds to a downward (positive) local velocity of the mixture in regions of the wave where the averaged volume fraction of particles is higher, which is a primary result of the horizontal motion of the particles. The other contribution, which does not affect the averaged volume fraction of particles, is a primary result of the rotational motion of the particles, which is emphasized in regions of large shear rate in the wave. The dispersion relation that determines the discrete eigenvalue $\hat{\sigma}$ is obtained by substituting (3.7) into (3.5), to yield

$$Re_L\hat{\sigma}+\hat{k}^2 = \frac{1}{2\pi}\int_{-\frac{\pi}{2}}^{\frac{\pi}{2}}\int_0^{\pi}\frac{[\hat{k}\,\hat{v}_{s,y}(\theta,\phi)]^2}{\hat{\sigma}^2+[\hat{k}\,\hat{v}_{s,y}(\theta,\phi)]^2}\,\sin\theta\,\mathrm{d}\theta\mathrm{d}\phi. \tag{3.8}$$

The term proportional to $\hat{v}_{s,y}$ in (3.7) does not contribute to the integral in (3.8) since it is an odd function of ϕ.

3.2. *Mode analysis for* $Re_L \ll 1$

First, let us consider the case $Re_L = 0$, as studied by Koch & Shaqfeh (1989). For $\hat{k} < 1$ there are two possible eigenvalues of the same magnitude, corresponding to growth and decay of the eigenfunctions respectively. Maximum growth/decay is obtained as $\hat{k} = 0$, for which $\hat{\sigma} = \pm\sqrt{3/5}$. In the limit $\hat{k} = 1$ the two eigenvalues merge at $\hat{\sigma} = 0$. (In fact, these limiting values of the growth rate and wavenumber satisfy the dispersion relation for any value of $Re_L > 0$.) For $\hat{k} > 1$ no eigenfunctions of the discrete spectra exist. (Koch & Shaqfeh 1989 also show the existence of continuous spectra of neutral, travelling waves, a feature not addressed in this work.)

In the present analysis, however, the dispersion relation for $Re_L = 0$ is not uniformly valid for all $\hat{k}$ as $Re_L \to 0$ in (3.8). For small Re_L the dispersion relation displays a boundary layer character for the eigenvalues $\hat{\sigma}$ close to $\hat{k} = 0$. The positive growth rate here also approaches zero as $\hat{k} \to 0$ and there is a maximum of the growth rate for a finite $\hat{k} \neq 0$. The asymptotic behaviour of (3.8) as $Re_L \to 0$ for small wavenumbers is obtained by introducing the scaled wavenumber $\bar{k} = \hat{k}/\sqrt{Re_L}$ into (3.8), to obtain

$$\hat{\sigma}+\bar{k}^2 = \frac{1}{2\pi}\int_{-\frac{\pi}{2}}^{\frac{\pi}{2}}\int_0^{\pi}\frac{[\bar{k}\,\hat{v}_{s,y}(\theta,\phi)]^2}{\hat{\sigma}^2+Re_L\,[\bar{k}\,\hat{v}_{s,y}(\theta,\phi)]^2}\,\sin\theta\,\mathrm{d}\theta\,\mathrm{d}\phi. \tag{3.9}$$

For $Re_L \to 0$ evaluation of the integral yields

$$\hat{\sigma}+\bar{k}^2 = \frac{3\bar{k}^2}{5\hat{\sigma}^2} \Leftrightarrow \bar{k}^2 = \frac{\hat{\sigma}^3}{\frac{3}{5}-\hat{\sigma}^2} \Leftrightarrow \hat{\sigma}^3+\bar{k}^2\hat{\sigma}^2-\frac{3}{5}\bar{k}^2 = 0, \tag{3.10}$$

which is valid for $\bar{k} \sim 1$ or smaller. For $\bar{k} \gg 1$ we retain the small wavenumber limit, $\hat{k} \to 0$, of the outer solution for $Re_L = 0$, i.e. $\hat{\sigma} = \pm\sqrt{3/5}$. For finite values of $\bar{k}$, however, the magnitudes of the positive and negative eigenvalues are not the same. In fact, for real roots of (3.10) and $\hat{\sigma}_+ > 0$ we must have $\hat{\sigma}_+^2 < 3/5$, whereas for $\hat{\sigma}_- < 0$ it must hold that $\hat{\sigma}_-^2 > 3/5$. Thus, the approximate dispersion relation

(3.10) may be evaluated by using $\hat{\sigma}$ as a parameter. If values of positive growth rates are taken to be in the interval $\hat{\sigma}_+ \in [0, \sqrt{3/5}]$ and negative growth rates in the interval $\hat{\sigma}_- \in [-\infty, -\sqrt{3/5}]$, then the corresponding values of $\bar{k}$ are obtained from the second equation of (3.10). In this manner, modes of positive growth rates are found distributed over all values of $\bar{k} \leqslant 1$. However, when evaluating these expressions for the negative growth rates one finds that there is a lower limit in the scaled wavenumber, $\bar{k}_t^2 = 9\sqrt{5}/10$, below which these non-travelling decaying eigenfunctions cease to exist. Above this limit there are, for each $\bar{k}$, two modes of negative, real eigenvalues, one of which has a magnitude of the order of the growth rate and the other one generally much larger, representing a quite rapidly decaying eigenfunction. For wavenumbers below this limit, i.e. $\bar{k} < \bar{k}_t$, the decaying eigenfunctions are instead travelling waves. To see the existence of the travelling waves we study (3.10) in the limit $\bar{k} \ll 1$, giving $\hat{\sigma}^3 \approx (3/5)\bar{k}^2$. This simplified equation has one real, positive root,

$$\hat{\sigma}_+ \approx (3\bar{k}^2/5)^{1/3}, \tag{3.11}$$

and two complex roots with negative growth rates, $\mathscr{S} = \hat{\sigma}_- + \mathrm{i}\hat{\omega}$, where

$$\hat{\sigma}_- \approx -\tfrac{1}{2}\hat{\sigma}_+, \quad \hat{\omega} \approx \pm\sqrt{3}/2\hat{\sigma}_+. \tag{3.12}$$

In general on the interval $\bar{k} \in [0, (9\sqrt{5}/10)^{1/2}]$, as one root of (3.10) is real, the two imaginary roots must be complex conjugates and can be expressed in terms of the positive real root of the non-travelling wave:

$$\hat{\sigma}_- = -\frac{1}{2}\left(\hat{\sigma}_+ + \frac{\hat{\sigma}_+^3}{\frac{3}{5} - \hat{\sigma}_+^2}\right), \quad \hat{\omega} = \pm\sqrt{|\mathscr{S}|^2 - \hat{\sigma}_-^2}, \quad |\mathscr{S}|^2 = \frac{\frac{3}{5}\hat{\sigma}_+^2}{\frac{3}{5} - \hat{\sigma}_+^2}, \tag{3.13}$$

where $\hat{\sigma}_+$ is the positive real root at the same $\bar{k}$ as given by (3.10). At the limiting wavenumber $\bar{k}_t^2 = 9\sqrt{5}/10 \approx 1.42^2$ we find $\hat{\omega} = 0$ and $\hat{\sigma}_t = -3/\sqrt{5}$, all according to (3.10).

The inner region, $\hat{k} \sim Re_L^{1/2}$, does not cover the location of the maximum growth rate versus $\hat{k}$. In order to capture this, a higher-order approximation of the integral on the right-hand side of (3.9) must be considered. Further, the location of the maximum scales as $\hat{k} \sim Re_L^{1/4}$, i.e. small, but larger values of $\hat{k}$ than covered by the inner scaling. We can verify this by introducing an intermediate scaling of the wavenumber, $\tilde{k} = \hat{k}/Re_L^{1/4}$, into (3.8), to get

$$Re_L^{1/2}\hat{\sigma} + \tilde{k}^2 = \frac{1}{2\pi}\int_{-\frac{\pi}{2}}^{\frac{\pi}{2}}\int_0^{\pi} \frac{\left[\tilde{k}\,\hat{v}_{s,y}(\theta,\phi)\right]^2}{\hat{\sigma}^2 + Re_L^{1/2}\left[\tilde{k}\,\hat{v}_{s,y}(\theta,\phi)\right]^2}\sin\theta\,\mathrm{d}\theta\mathrm{d}\phi. \tag{3.14}$$

By expanding the integrand in powers of $Re_L^{1/2}$ and evaluating the resulting integrals for the first two terms of the expansion, one obtains

$$Re_L^{1/2}\hat{\sigma} + \tilde{k}^2 = \frac{3\tilde{k}^2}{5\hat{\sigma}^2} - Re_L^{1/2}\frac{27\tilde{k}^4}{35\hat{\sigma}^4} + O(Re_L). \tag{3.15}$$

Thus, to lowest order we see that $\hat{\sigma} \approx \pm\sqrt{3/5}$, and we introduce the following expansion for the growth rate:

$$\hat{\sigma} = \pm(\sqrt{3/5} - Re_L^{1/2}\tilde{\sigma}_1(\tilde{k})) + O(Re_L). \tag{3.16}$$

The negative sign applies to the upper branch of the two negative growth rates. Collecting terms of order $Re_L^{1/2}$ in (3.15) gives

$$\tilde{\sigma}_1 = \pm\tfrac{3}{10}\tilde{k}^{-2} + \tfrac{27}{70}\left(\tfrac{3}{5}\right)^{-3/2}\tilde{k}^2, \tag{3.17}$$

where the positive sign is still for the positive growth rate. The maximum growth rate is obtained at

$$\hat{k}_{max} = Re_L^{1/4}\tilde{k}_{max} = Re_L^{1/4}\left(\tfrac{35}{27}\right)^{1/4}\left(\tfrac{3}{5}\right)^{5/8} \approx Re_L^{1/4}0.7754, \tag{3.18}$$

where

$$\begin{aligned}\hat{\sigma}_{max} &= \sqrt{3/5} - Re_L^{1/2}\tilde{\sigma}_{1,max} \\ &= \sqrt{3/5} - Re_L^{1/2}\sqrt{\tfrac{27}{35}}\left(\tfrac{5}{3}\right)^{1/4} \approx 0.7746 - Re_L^{1/2}0.9980.\end{aligned} \tag{3.19}$$

In matching this intermediate region with the inner region one identifies

$$\hat{\sigma}_{c.p.} = \pm\sqrt{3/5} - Re_L^{1/2}\tfrac{3}{10}\tilde{k}^{-2} = \pm\sqrt{3/5} - \tfrac{3}{10}\overline{k}^{-2} \tag{3.20}$$

as the common part of the two expansions. Therefore, an expansion uniformly valid for $\hat{k} \sim Re_L^{1/4}$ or smaller is given by

$$\hat{\sigma}_{uniform} = \hat{\sigma}_{inner} + \hat{\sigma}_{intermed} - \hat{\sigma}_{c.p.}. \tag{3.21}$$

For larger wavenumber, $\hat{k}/Re_L^{1/4} \gg 1$ and $Re_L \to 0$, the dispersion relation is close to that for $Re_L = 0$ of the two upper branches of $\hat{\sigma}$. We can obtain a first-order correction of the form

$$\hat{\sigma} = \hat{\sigma}_0(\hat{k}) + Re_L\hat{\sigma}_1(\hat{k}) + O(Re_L^2), \tag{3.22}$$

where $\hat{\sigma}_1(\hat{k}) \leqslant 0$ is the same function for both branches of $\hat{\sigma}_0$. However, the procedure to obtain $\hat{\sigma}_1$ is as complicated as to consider the full dispersion relation, and is not followed here. We can just conclude that $\hat{\sigma}_1(\hat{k} = 1) = 0$. The lowest branch, with rapidly decaying eigenfunctions, has no counterpart in the case $Re_L = 0$. For this branch (3.10) applies also for $\hat{k}/Re_L^{1/2} \gg 1$ as $Re_L \to 0$, so that $\hat{\sigma} \approx -\hat{k}^2/Re_L$. In fact, this approximation is also valid for the lowest branch for $Re_L \sim 1$ if $\hat{k} \gg 1$.

3.3. *General mode analysis*

In the general case, for arbitrary Re_L, we can evaluate the integral on the right-hand side of (3.8) numerically. But first, the integration with respect to the azimuthal angle ϕ can be performed analytically by a contour integration around the unit circle in the complex plane. By introducing the abbreviation

$$\Omega(\theta) = \frac{\hat{\sigma}/\hat{k}}{\dfrac{3}{2}\sin^2\theta}, \tag{3.23}$$

(3.8) can be written

$$Re_L\hat{\sigma} + \hat{k}^2 = \frac{1}{2}\int_0^{\pi} \sin\theta\, J(\theta)\mathrm{d}\theta, \tag{3.24}$$

where

$$J(\theta) = \frac{1}{\pi}\int_{-\frac{\pi}{2}}^{\frac{\pi}{2}} \frac{\sin^2 2\phi}{[\Omega(\theta)]^2 + \sin^2 2\phi}\,\mathrm{d}\phi = \frac{\mathrm{i}}{2\pi}\oint_{|z|=1} \frac{(z^2-1)^2}{z[(2\Omega)^2 z^2 - (z^2-1)^2]}\,\mathrm{d}z, \quad (3.25)$$

and where the variable transformation leading to the second integral in (3.25) is defined by $z = \mathrm{e}^{\mathrm{i}2\phi}$. The integrand of the last expression has three poles within the unit circle, and we obtain

$$J(\theta) = 2\left(1 - \frac{1}{z_p^2 + 1}\right), \quad z_p = \Omega(\theta) - \sqrt{1 + [\Omega(\theta)]^2}. \quad (3.26)$$

Now, the integral over the polar angle in (3.24) can be evaluated numerically for any specified value of the ratio $\chi = \hat{\sigma}/\hat{k}$. Equation (3.24) then defines a second-order equation for the corresponding value of $\hat{k}$, where the positive root is chosen. At last, $\hat{\sigma}$ is given by $\chi\hat{k}$, where χ can be taken as any positive or negative value to cover both growing and decaying modes.

4. Results

The dispersion relation for non-travelling modes as evaluated from (3.23), (3.24) and (3.26) is shown in figure 2 for Reynolds numbers in the range 10^{-5}–4. This gives an overview of the growth rates of these modes for different Re_L and non-dimensional wavenumbers $\hat{k}$. As $\hat{k} < 1$ there is always one growing mode and two decaying modes for each of the Re_L chosen for evaluation. However, depending on the magnitude of Re_L, there is a value of $\hat{k}$ below which the decaying modes are travelling waves. (The travelling modes are shown in figure 3 only.) As Re_L is small this critical wavenumber is $\hat{k} \approx 1.42 Re_L^{1/2}$. For $\hat{k} > 1$ the single non-travelling mode for each Re_L has negative growth rate. As $Re_L \ll 1$, the modes of the two upper branches are close to the case $Re_L = 0$, except in a region close to $\hat{k} = 0$. For the four lowest Reynolds numbers displayed, the negative growth rates are complemented with the uniformly valid asymptotic solution (3.21), uniformly valid for $\hat{k} \sim Re_L^{1/4}$ and smaller.

Figure 3 illustrates the inner region of the dispersion relation, as $\hat{k} \sim Re_L^{1/2}$ and $Re_L \to 0$. The approximate asymptotic growth rates, (3.10), versus the inner scaling of the wavenumber, $\hat{k}/Re_L^{1/2}$, are here compared to the numerical evaluation of the exact dispersion relation at different Re_L. The numerical evaluation covers the same data as presented in figure 2, the only difference being the scaling of the wavenumber. The exact dispersion relations for $Re_L = 10^{-5}, 10^{-4}, 10^{-3}$ are seen to collapse well into the single curve of the asymptotic relation, whereas for $Re_L \geqslant 10^{-2}$ there are significant departures. The rapidly decaying mode in the lower part of the diagram collapses for all Re_L as $\hat{k}/Re_L^{1/2}$ is large enough. The rate of decay of the travelling mode and its frequency (insert) in the region $\hat{k}/Re_L^{1/2} \leqslant 1.42$ are also indicated in figure 3 using the asymptotic solution (3.13).

As previously mentioned, the inner region does not cover the location of maximum growth rate. The maximum is instead apparent when presenting the solution in terms of the intermediate scaling of the wavenumber and growth rate as shown in figure 4. The asymptotic solution is here according to (3.17) and is compared to the exact dispersion relation for small Re_L. For these small Reynolds numbers the position of the maximum is well described by the asymptotic result (3.18) as indicated by the graph.

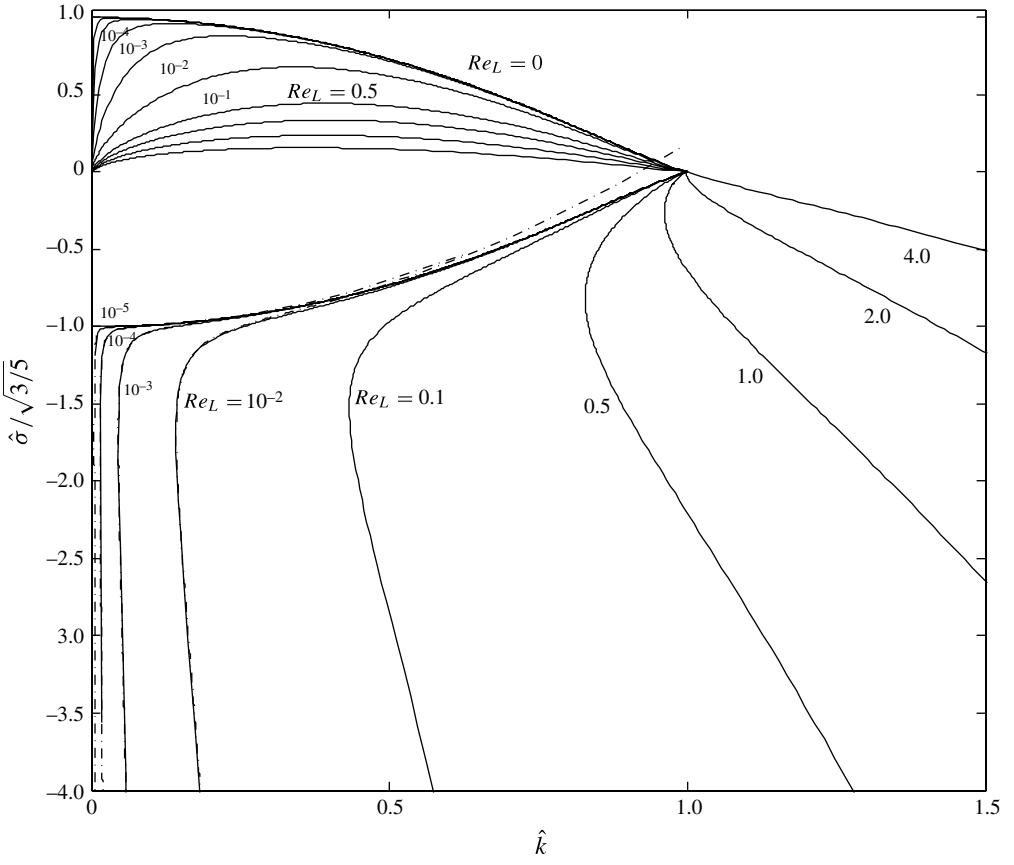

FIGURE 2. Overview of the dispersion relation for non-travelling linear eigenmodes for different Re_L. Numerical evaluation of the exact dispersion relation (—), asymptotic expression for small Re_L (decaying modes only) according to (3.21) (– · –).

A complete graph of the growing mode versus $\hat{k}$ is shown in figure 5. The path of maximum growth rate for different Reynolds numbers according to the asymptotic solution is indicated by the dashed line, which agrees well with the maximum of the exact dispersion relation for small Re_L. Dash-dotted lines show the dispersion relation in terms of the approximate asymptotic solution (3.21), which captures well the exact solution for small $\hat{k}$ as the Reynolds number is not too large. The limiting dispersion relation for $Re_L = 0$, as previously reported by Koch & Shaqfeh (1989), is also included in the graph, for which the maximum growth appears for $\hat{k} = 0$. Thus, a major difference in the result of the present theory compared to that of Koch & Shaqfeh (1989) is that the maximum growth rate here appears at a finite wavelength. In the insert of figure 5 we show the growth rate versus the logarithm of the inverse wavenumber. For the smallest Reynolds numbers one then finds that the peak is surrounded by a plateau of almost indifferent growth rate in a rather wide region of wavelengths, before the cut-off sets in at the longest wavelengths.

To test the relevance of the present results from linear stability theory, we make a comparison with the experiments of Metzger *et al.* (2007*a*). From their particle image velocimetry (PIV) measurements they report alternating structures of vertical flow that

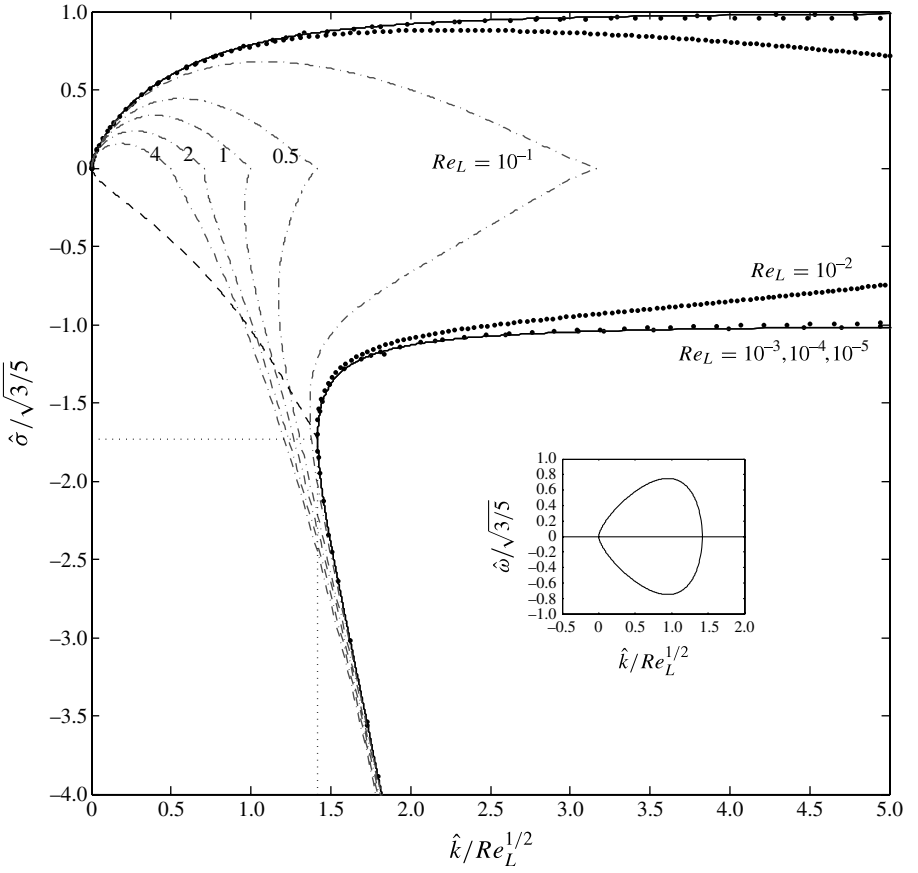

FIGURE 3. Graph of dispersion relation using the inner scaling of the wavenumber. Asymptotic expression (3.10) for $\hat{\sigma}$ of non-travelling (—) and travelling (− −) eigenmodes of the inner region. Numerical evaluation of the exact dispersion relation for non-travelling eigenmodes at $Re_L = 10^{-5}, 10^{-4}, 10^{-3}, 10^{-2}$ (•), and at $Re_L = 10^{-1}, 0.5, 1.0, 2.0, 4.0$ (− · −). The inserted figure shows the frequency, $\hat{\omega}$, of the travelling modes. The upper limit in the wavenumber of the decaying travelling eigenmodes, $\hat{k}_t$, and the corresponding negative growth rate (· · ·).

span the height of a vessel filled with a sedimenting suspension of rigid fibres. An average of the horizontal correlation length for the vertical velocity of these structures and its development with time is given for some different cases. The correlation length λ_C is determined from the instantaneous locations of an observed negative minimum in the horizontal velocity correlation function computed along different lines on the PIV flow field map. The average of these locations is taken as the instantaneous correlation length. As the minima correspond to a negative velocity correlation, this length represents half a wavelength of a periodic disturbance, $\lambda_C = \lambda/2$.

Five different particles, denoted by A–E, are used in their experiments as given in table 1. Data of the different fluids used, denoted by 1–4, are given in table 2. (For more detailed information on the experimental data see Metzger *et al.* 2007*a*.) We have used their experimental data to evaluate the wavelength of the maximum growth rate according to the present theory and compared that to their measured correlation length data, $2\lambda_C$. In a first set of experiments of different vessel size they conclude

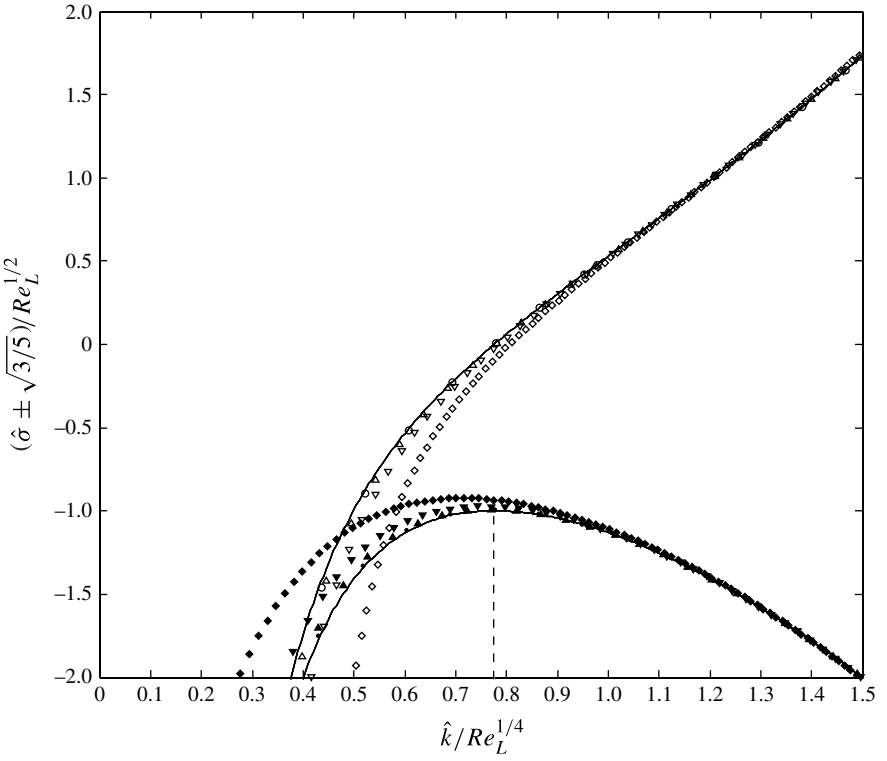

FIGURE 4. Graph of dispersion relation using the intermediate scaling of the wavenumber. Asymptotic expression (3.17) of $-\tilde{\sigma}_1$ for the two modes of largest growth rate (−), where the curve with a peak refers to the growing mode. Numerical evaluation of growth rate at $Re_L = 10^{-5}(\circ), 10^{-4}(\triangle), 10^{-3}(\triangledown), 10^{-2}(\diamond)$. Growing mode in filled symbols. Upper branch of decaying modes in open symbols.

Particle	ρ_D (g cm^{-3})	l (mm)	r
A	1.13	1.52	11
B	−〃−	2.96	10
C	−〃−	6.12	44
D	−〃−	8.72	16
E	8.9	2.08	13

TABLE 1. Experimental particle data of Metzger *et al.* (2007*a*).

that the width of the vessel sets an upper limit to the double correlation length. Flow structures of this type that are of larger scale than this cannot develop according to the experiments.

There are two other series of experiments reported that are more relevant for a comparison. First the effect of particle volume fraction is investigated in a container of horizontal dimensions $130 \times 52\,(l/2)^2$ using a combination of particle A and fluid 2. The volume fraction is varied from $\alpha_0 = 0.1 - 1\,\%$ as specified in table 3. The corresponding Reynolds numbers, $Re_L \sim 10^{-5}$, and the scaled wavelengths of

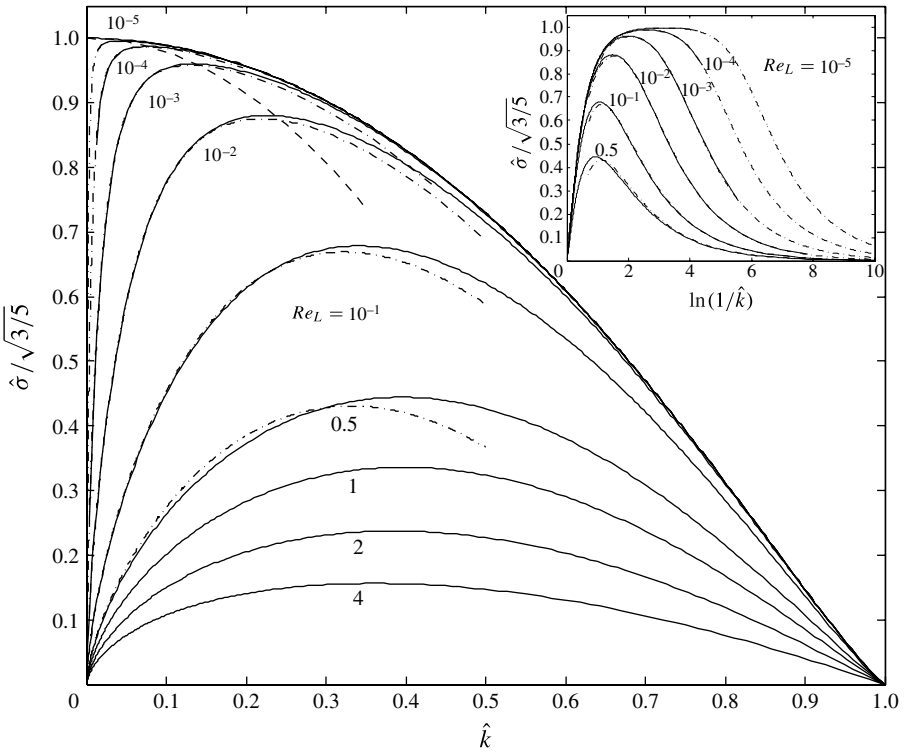

FIGURE 5. Graph of dispersion relation for growing modes only. Numerical evaluation of the exact dispersion relation for linear eigenmodes for different values of $Re_L(-)$, asymptotic expression of the dispersion relation according to (3.21) for values of $Re_L \leqslant 0.5$ $(- \cdot -)$, locus of maximum growth rate according to the asymptotic analysis for small $Re_L(--)$. The insert shows the same data but versus the logarithm of the inverse wavenumber to illustrate the wavelength selection.

Fluid	ρ_C (g cm^{-3})	μ (Pa s)
1	0.96	0.10
2	1.03	0.13
3	1.02	0.05
4	1.04	0.36

TABLE 2. Experimental fluid data of Metzger *et al.* (2007*a*).

maximum growth rate, $\lambda_{max}/(l/2)$, as calculated from (3.18) are also given in the table. The last column of table 3 indicates the reported measured values of the double correlation lengths, $2\lambda_C/(l/2)$. Independent of volume fraction, the measurements show that $2\lambda_C/(l/2)$ decreases with time from $\approx$120 (i.e. slightly below 130, the scaled width of the container) down to $\approx$70. Our results for the wavelengths of maximum growth were indeed within this range for the three smallest volume fractions considered. For the three largest values of the volume fraction our predictions for λ_{max} are lower than the measured range. This was the result of a trend in the theory which predicted a decrease of $\lambda_{max}/(l/2)$ with volume fraction as $\sim\alpha_0^{-1/4}$ as indicated in the

Batch	$\alpha_0 \times 10^2$	$Re_L \times 10^4$	$\lambda_{max}/(l/2)$	$2\lambda_C/(l/2)$
A + 2	0.1	0.220	111	70–120
A + 2	0.2	0.150	86	–〃–
A + 2	0.3	0.130	74	–〃–
A + 2	0.5	0.098	61	–〃–
A + 2	0.7	0.082	54	–〃–
A + 2	1.0	0.069	47	–〃–

TABLE 3. Comparison of present theory and experiments of Metzger *et al.* (2007*a*) for different volume fractions.

Batch	$\alpha_0 \times 10^2$	$Re_L \times 10^4$	λ_{max}/W	$2\lambda_C/W$
A + 2	0.5	0.1	0.23	0.2–0.5
A + 3	0.5	0.7	0.14	–〃–
B + 2	0.5	0.9	0.28	–〃–
C + 2	0.5	0.3	0.25	–〃–
D + 2	0.5	8.8	0.34	–〃–
D + 4	0.5	1.0	0.57	–〃–
E + 4	0.5	1.2	0.13	–〃–

TABLE 4. Comparison of present theory and experiments of Metzger *et al.* (2007*a*) for different fluids and particles.

insert of figure 6. One should bear in mind, though, that the theory did not account for any kind of particle interactions, the effects of which should increase with volume fraction. The experiment at 0.5 % volume fraction in table 3 was also performed in a cell of a wider dimension, $260 \times 52\,(l/2)^2$, with essentially the same result for the correlation length. However, in a more narrow container, $52 \times 52\,(l/2)^2$, the measured structures were reported to be constrained by the width of the cell. This is also consistent with the result of the present theory for which the most unstable wavelength is 61 $(l/2)$, i.e. larger than the cell width at 52 $(l/2)$. In figure 6 we show the growth rate peak of the linear theory versus the scaled wavenumber $\lambda/(l/2)$ for the different volume fractions considered in the experiments of Metzger *et al.* (2007*a*). We see that the range of experimental data for the double correlation length falls well within the plateau of almost indifferent growth rate even for the larger volume fractions.

The second set of experiments by Metzger *et al.* (2007*a*) chosen for comparison investigates the effect of different particles and fluids using a constant volume fraction of $\alpha_0 = 0.5\,\%$ and a vessel of horizontal cross-section 20×4 cm^2. The different combinations of fluid and particle data used are summarized in table 4. According to Metzger *et al.* (2007*a*) all the curves from the experiments of the double correlation length versus time decrease from a value of about $0.5W$ to $0.2W$, where $W = 20$ cm is the width of the vessel. Thus, in this case the length scale of the streaming columns are substantially less than the width of the vessel. The corresponding values of λ_{max}/W from the linear theory are also given in table 4. Except for the cases A + 3, E + 4 and D + 4 the theoretical values fall within the range of experimental data. Figure 7 shows our predicted growth rates versus the scaled wavenumber for the batches considered in table 4. The measured range of the double correlation lengths of the streaming columns reported roughly matches all the plateaus of indifferent growth

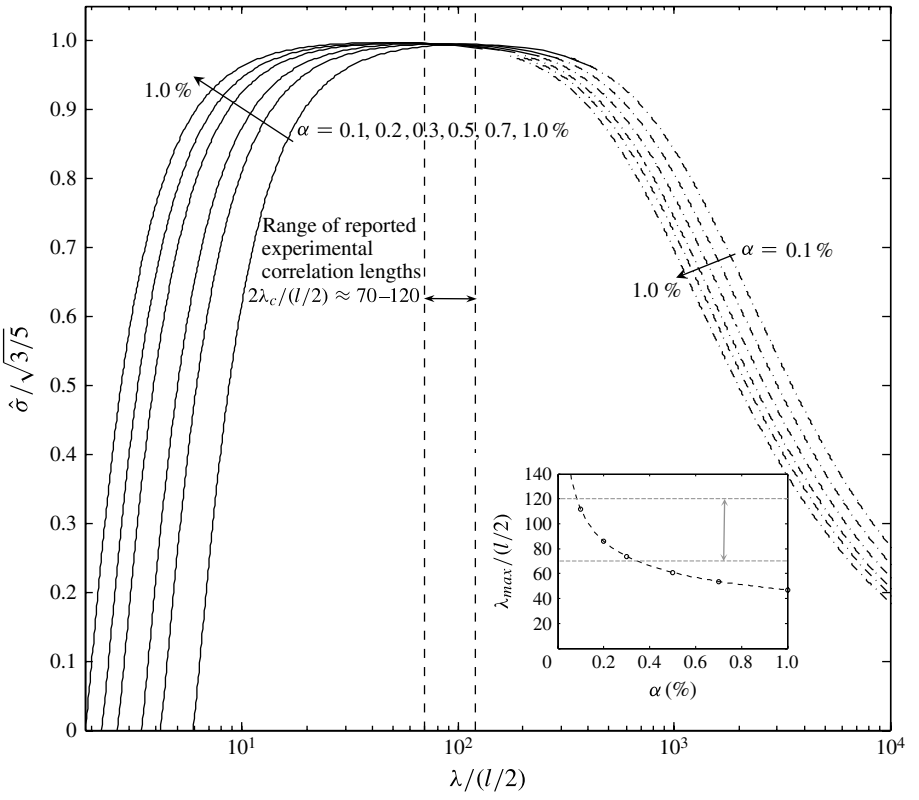

FIGURE 6. Growth rate versus the scaled wavelength calculated from the present theory using data from the experimental conditions investigated by Metzger *et al.* (2007*a*) as specified by tables 1–3. Numerically evaluated part of the exact dispersion relation (—), asymptotic expression for the dispersion relation at larger wavelengths (− · −). The upper and lower limits of the measured double correlation lengths (− −) are also indicated in the figure. The inserted figure shows the wavelength with the maximum growth rate versus the volume fraction according to linear theory (− −).

rates, although predictions for batches A + 3, E + 4 and D + 4 are truly at the limits of the measured range.

5. Conclusions

We considered the instability of a dilute, initially homogeneous suspension of spheroids or rods settling due to gravity in an infinite environment. The mathematical formulation was based on the mixture theory for two-phase flow, where the motion of the particles relative to the mixture is given by an algebraic relation based on the settling velocity of a particle under Stokes flow conditions. For the particular case of horizontal wavenumbers, the equations derived governing the linear instability extended the theory of Koch & Shaqfeh (1989) by including also the small, but non-zero, inertia of the bulk motion. The Reynolds number, describing the relative importance of the bulk inertia, was given by $Re_L = V_s L/\nu_C$, where V_s is a measure of the settling speed and L is the length scale on which buoyancy and viscous forces balance in the bulk. The resulting dispersion relation for eigenvalues of the discrete spectra at a fixed $Re_L \neq 0$ (no matter how small) showed that in the limit

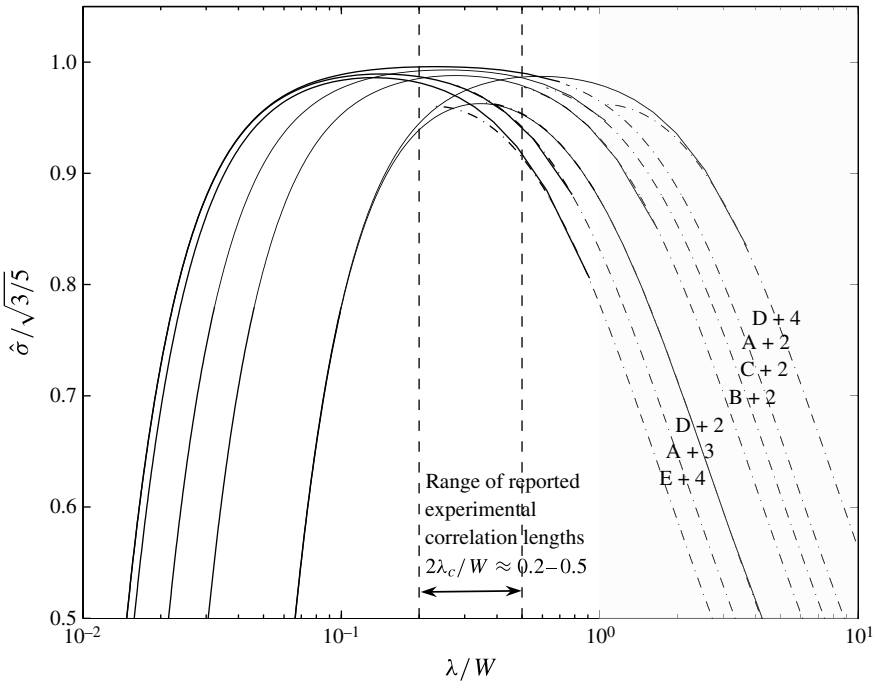

FIGURE 7. Growth rate versus the normalized wavelength calculated from the present theory using data from the different batches investigated experimentally by Metzger *et al.* (2007*a*) as specified by tables 1, 2 and 4. Numerically evaluated part of the exact dispersion relation (—), asymptotic expression for the dispersion relation at larger wavelengths (— · —). The upper and lower limits of the measured double correlation lengths (– –) are also indicated in the figure. The shaded area corresponds to wavelengths larger than the experimental vessel width.

of large wavelengths eigenvalues of positive growth rate approach zero as $\lambda^{-2/3}$, and that the largest growth rate is obtained at a finite wavelength. This is in contrast to the previous theory of Koch & Shaqfeh (1989) at $Re_L = 0$, who found the largest growth rate for infinitely long waves. (On the other hand, for any fixed finite wavelength, no matter how large, the results of the present growth rate do agree with that of Koch & Shaqfeh (1989) as the Reynolds number approaches zero.) For small values of the bulk Reynolds number, $Re_L \ll 1$, we found an approximate, asymptotic solution for the dispersion relation between growth rate and wavenumber. From this it was shown that the wavelength of maximum growth is given by $\lambda_{max} \approx 2.5\pi L\, Re_L^{-1/4} \approx 0.9d\sqrt{\ln(2r)/\alpha_0}\, Re_L^{-1/4}$, where the last expression is for slender particles with $r \gg 1$. (Note that $Re_L \ll 1$ also depends on α_0 and r.) Thus, λ_{max} should be the typical length scale of structures in the early development of vertical streamers as experimentally reported.

It should be noted that the effect of inertia here does not refer to the inertia of the local relative flow of the particle and fluid. The fibres' tendency to align in the shear flow is still given by the Stokesian limit, instantaneously following the changes of the bulk shear flow. The main effect of inertia here is rather on the set-up of the shear flow itself. At long wavelengths of a density perturbation, the time scale needed to set up a viscously dominated flow, λ^2/ν, is much longer than for perturbations of shorter wavelength. As this viscous set-up time is completely neglected in a theory assuming $Re_L = 0$, long wavelengths, such that the viscous set-up time is

of the order of the settling time or larger, i.e. $\lambda^2/\nu > L/V_s$, are then not correctly reproduced. Or equivalently, in non-dimensional terms, inertial effects will be of major importance if $(\lambda/L)^2 > Re_L^{-1}$. At small, but non-zero Re_L, this represents a regime of small wavenumbers which is not captured correctly by the theory at $Re_L = 0$. This is typical for a singular perturbation problem where a small parameter, here the Reynolds number, multiplies the highest-order derivative of an equation, in our case the time derivative in the momentum equation. With the present theory at $Re_L \neq 0$, there is no such inconsistency, where instead the early development of a long wavelength density perturbation is dictated by an inertial force balance, which limits the rate of increase of the columnar flow. Another way of putting it is that at long wavelengths, the fibres indeed have a long way to travel in the horizontal direction to be collected in a streamer, as required by the instability mechanism. With the assumption $Re_L = 0$, this is instantaneously compensated for by a large shear rate which acts to align the fibres efficiently in the most advantageous direction, and thereby reinforces the instability (whereas at short enough wavelengths fibres aligned in the shear flow quickly pass a streamer region and the instability is damped). However, according to the present theory at $Re_L \neq 0$, the longer travel distance at longer wavelengths is not fully compensated for, as the process of setting up the magnitude of the shear rate is delayed by the inertia of the columnar flow in these longer waves.

To test our hypothesis we compared the computed values of λ_{max} with the measured correlation lengths obtained by Metzger *et al.* (2007*a*) in a series of PIV experiments. The peak location of the computed theoretical growth rate versus wavelength matched for most batches the measured range of the double correlation lengths of the streaming columns reported in the PIV experiments. In summary, there is no evident contradiction between the results of the present theory and those of the reported experiments. In fact, the agreement is surprisingly good, although the theory did not give a sharp cut for the growth of longer wavelengths. However, one may note that, according to Metzger *et al.* (2007*a*), the measured correlation length is the average of a 'smooth but wide distribution' of the location of the correlation minima at a given time. In fact the dispersion in correlation length is given to be approximately 50 %. At best, this might be taken as an experimental verification of the rather wide plateau of large growth rates predicted by the present theory at small Re_L, as clearly visualized in the presented graphs. The relative width of the plateau region at small Re_L may be approximated from a formal quadrature approximation of the dispersion relation close to the maximum as $\Delta\lambda/\lambda_{max} \approx \Delta k/k_{max} \approx 0.62\ \sqrt{\Delta\sigma/\sigma_{max}}\, Re_L^{-1/4}$, where $\Delta\sigma \ll \sigma_{max}$ is a chosen maximum deviation in the plateau region. It is quite clear though, from tables 3 and 4, that the peak location of this plateau is less than the vessel width for all batches. Also, in the batches of figure 7, wavelengths of the vessel size have growth rates essentially lower than the maximum growth rate, which correlates well with the experimental results for these batches.

We also found two eigenmodes of negative growth rates. At small enough wavenumbers, $\hat{k} < 1.42 Re_L^{1/2}$, these decaying modes were travelling waves. Decaying modes may be of importance for a study of more general initial conditions of the density perturbation and its eventual nonlinear evolution. The linear combination of growing and decaying eigenfunctions can lead to transient growth, which may carry the perturbation into the nonlinear regime of development. Such phenomena may be part of an explanation for the experimentally observed development in time of the correlation length as measured by Metzger *et al.* (2007*a*). The effects of the vessel walls were not considered in this work. However, for a more detailed comparison with

the experimental result, e.g. regarding the time development just mentioned, at least the vertical walls should be accounted for. Work on the nonlinear evolution of the present formulation and inclusion of the vertical container walls is in progress.

Acknowledgements

This work was supported by the Swedish Research Council (VR).

REFERENCES

BATCHELOR, G. K. 1970 Slender-body theory for particles of arbitrary cross-section in Stokes flow. *J. Fluid Mech.* **44**, 419–440.

BUTLER, J. E. & SHAQFEH, E. S. G. 2002 Dynamic simulations of the inhomogeneous sedimentation of rigid fibres. *J. Fluid Mech.* **468**, 205–237.

GUAZZELLI, É. & HINCH, J. 2011 Fluctuations and instability in sedimentation. *Annu. Rev. Fluid Mech.* **43**, 97–116.

HAPPEL, J. & BRENNER, H. 1965 *Low Reynolds Number Hydrodynamics*. Prentice-Hall.

HERZHAFT, B. & GUAZZELLI, É 1999 Experimental study of the sedimentation of dilute and semi-dilute suspensions of fibres. *J. Fluid Mech.* **384**, 133–158.

HERZHAFT, B., GUAZZELLI, É, MACKAPLOW, M. B. & SHAQFEH, E. S. G. 1996 Experimental investigation of the sedimentation of a dilute fibre suspension. *Phys. Rev. Lett.* **77** (2), 290–293.

ISHII, M. 1975 *Thermo-Fluid Dynamic Theory of Two-Phase Flow*. Eyrolles.

JEFFREY, G. B. 1922 The motion of ellipsoidal particles immersed in a viscous fluid. *Proc. R. Soc.* **A102**, 161–179.

KOCH, D. L. & SHAQFEH, E. S. G. 1989 The instability of a dispersion of sedimenting spheroids. *J. Fluid Mech.* **209**, 521–542.

KUMAR, P. & RAMARO, B. V. 1991 Enhancement of the sedimentation rates in fibrous suspensions. *Chem. Engng Commun.* **108**, 381–401.

KUUSELA, E., LAHTINEN, J. M. & ALA-NISSILA, T. 2005 Collective effects in settling of spheroids under steady-state sedimentation. *Phys. Rev. Lett.* **90**, 094502.

MACKAPLOW, M. B. & SHAQFEH, E. S. G. 1998 A numerical study of the sedimentation of fibre suspensions. *J. Fluid Mech.* **376**, 149–182.

METZGER, B., BUTLER, J. E. & GUAZZELLI, É 2007*a* Experimental investigation of the instability of a sedimenting suspension of fibres. *J. Fluid Mech.* **575**, 307–332.

METZGER, B., BUTLER, J. E. & GUAZZELLI, É 2007*b* On wavelength selection by stratification in the instability of settling fibres. *Phys. Fluids* **19**, 098105.

METZGER, B., GUAZZELLI, É & BUTLER, J. E. 2005 Large-scale streamers in the sedimentation of a dilute fibre suspension. *Phys. Rev. Lett.* **95**, 164506.

NARSIMHAN, V. & SHAQFEH, E. S. G. 2010 Lateral drift and concentration instability in a suspension of bubbles induced by Marangoni stresses at zero Reynolds number. *Phys. Fluids* **22**, 101702.

SAINTILLIAN, D., DARVE, E. & SHAQFEH, E. S. G. 2005 A smooth particle-mesh Ewald algorithm for Stokes suspension simulations: the sedimentation of fibres. *Phys. Fluids* **17**, 033301.

SAINTILLIAN, D., SHAQFEH, E. S. G. & DARVE, E. 2006*a* The growth of concentration fluctuations in dilute dispersions of orientable and deformable particles under sedimentation. *J. Fluid Mech.* **553**, 347–388.

SAINTILLIAN, D., SHAQFEH, E. S. G. & DARVE, E. 2006*b* The effect of stratification on the wavenumber selection in the instability of sedimenting spheroids. *Phys. Fluids* **18**, 121503.

SHIN, M., KOCH, D. L. & SUBRAMANIAN, G. 2009 Structure and dynamics of dilute suspensions of finite-Reynolds number settling fibres. *Phys. Fluids* **21**, 123304.

TORNBERG, A.-K. & GUSTAVSSON, K. 2006 A numerical method for simulations of rigid fibre suspensions. *J. Comput. Phys.* **215**, 172–196.

UNGARISH, M. 1993 *Hydrodynamics of Suspensions*. Springer.